Periodically forced self-organization in the long-term evolution of planktic foraminifera

Andreas Prokoph, Anthony D. Fowler, and R. Timothy Patterson

Abstract: Wavelet transform and other signal analysis techniques suggest that the planktic foraminiferal (PF) long-term evolutionary record of the last 127 Ma can be attributed to complex periodic and nonlinear patterns. Correlation of the PF extinction pattern with other geological series favors an origin of the ~30 Ma periodicity and self-organization by quasi-periodic mantle-plume cycles that in turn drive episodic volcanism, CO_2-degassing, oceanic anoxic conditions, and sea-level fluctuations. Stationary ~30 Ma periodicity and a weak secular trend of ~100 Ma period are evident in the PF record, even without consideration of the mass extinction at the K–T boundary. The 27–32 Ma periodicity in the impact crater record and lows in the global sea-level curve, respectively, are ~6.5 Ma and ~2.3 Ma out of phase with PF-extinction data, although major PF-extinction events correspond to the bolide impacts at the K–T boundary and in late Eocene. Another six extinction events correspond to abrupt global sea-level falls between the late Albian and early Oligocene. Self-organization in the PF record is characterized by increased radiation rates after major extinction events and a steady number of baseline species. Our computer model of long-term PF evolution replicates this SO pattern. The model consists of output from the logistic map, which is forced at 30 Ma and 100 Ma frequencies. The model has significant correlations with the relative PF-extinction data. In particular, it replicates singularities, such as the K–T event, nonstationary 2.5–10 Ma periodicities, and phase shifts in the ~30 Ma periodicity of the PF record.

Résumé : La transformation d'ondelettes et d'autres techniques d'analyse de signaux suggèrent que l'évolution à long terme du plancton foraminifère (PF) des dernières 127 Ma puisse être attribué à des patrons non linéaires, périodiques et complexes. La corrélation du patron d'extinction du PF à d'autres séries géologiques plaide en faveur d'une origine de la périodicité ~30 Ma et une auto-organisation par ces cycles quasi périodiques de panache du manteau qui, à leur tour, sont responsables de volcanisme épisodique, de dégazage du CO_2, de conditions océaniques anoxiques et de fluctuations du niveau de la mer. Une périodicité stationnaire ~30 Ma et une faible tendance séculaire ~100 Ma sont évidentes dans le PF même si l'on ne tient pas compte de l'extinction massive à la limite K–T. La périodicité 27–32 Ma dans les enregistrements du cratère d'impact et les creux dans la courbe du niveau global de la mer sont, respectivement, déphasés de ~6,5 Ma et ~2,3 Ma par rapport aux données d'extinction du PF, bien que les événements majeurs d'extinction du PF correspondent aux impacts de bolides à la limite K–T et durant l'Éocène tardif. Six autres événements d'extinction correspondent à des chutes abruptes du niveau global de la mer entre l'Albien tardif et l'Oligocène précoce. L'auto-organisation (SO) du PF est caractérisée par une augmentation des taux de radiation après les événements d'extinction majeurs ainsi qu'un nombre constant d'espèces de base. Notre modèle informatique de l'évolution à long terme du PF redonne ce patron de SO. Le modèle consiste en des intrants tirés de la carte logistique, laquelle a été forcée à des fréquences de 30 et 100 Ma. Le modèle présente des corrélations importantes avec les données d'extinction relatives au PF. En particulier, il donne les points singuliers tels que l'événement K–T, des périodicités non stationnaires de 2,5 à 10 Ma et des déphasages dans la périodicité de ~30 Ma du PF.

[Traduit par la Rédaction]

Introduction

The interpretation of the geological record of evolution has been debated for more than a century. Two major hypotheses for macroevolution have been supported in the last three decades: gradualism, which naturally arose from the ideas of Darwin (1859), and "punctuated equilibrium." The latter hypothesis assumes very rapid evolution at distinct ecological regimes (Eldredge and Gould 1972). Background and mass extinction phenomena are an integral part of both evolutionary scenarios. Mass extinction, the focus of this research, has been analyzed in the context of these hypothesis, with two competing explanations being put forward.

(1) Evolution, and in particular mass extinction, is mostly triggered by variations of 26–33 Ma period within the intraterrestrial regime or from extraterrestrial impacts. Examples

Received November 26, 1999. Accepted April 7, 2000. Published on the NRC Research Press Web site on January 26, 2001. Paper handled by Associate Editor B. Chatterton.

A. Prokoph and A.D. Fowler[1]. Ottawa–Carleton Geoscience Centre and Department of Earth Sciences, University of Ottawa, P.O. Box 450, Stn. A, Ottawa, ON K1N 6N5, Canada.
R.T. Patterson. Ottawa–Carleton Geoscience Centre and Department of Earth Sciences, Carleton University Ottawa, Ottawa, ON K1S 5B6, Canada.

[1]Corresponding author (e-mail: afowler@science.uottawa.ca).

 DOI: 10.1139/cjes-38-2-293

of intraterrestrial evolutionary drivers include flood basalt volcanism, plate tectonics, and Earth's magnetic field reversals (Stothers 1986, 1993). Patterns in marine extinctions can be linked to the fluctuation and spreading of an oxygen minimum zone, i.e., during oceanic anoxic events (Brasier 1988). Hart (1990) postulated a periodicity of about 27 Ma for the planktic foraminiferal (PF) record by inspecting the reoccurrence of four distinct drops in PF origination. Possible extraterrestrial causes include asteroid or cometary showers due to movement of the Earth in the solar system and the galaxy (Rampino and Stothers 1984; Rampino and Caldeira 1992; Raup 1992).

(2) Evolution, especially the pattern of extinction and origination, is self-organized (Bak and Sneppen 1993; Kauffman 1993; Patterson and Fowler 1996; Sole et al. 1997). Self-organization (SO) describes, in dynamic systems theory, that complicated systems are reduced to a few collective degrees of freedom (Bak et al. 1988). For instance, small internal instabilities in highly cross-linked ecosystems may cause an "avalanche" of collapses of other taxa living in the interconnected community and possibly extinction of highly specialized taxa worldwide, leaving a few more-resistant forms (Plotnick and McKinney 1993). Broad swells of habitat are opened up for these more-resistant "generalist" forms. New species rapidly originate from these "generalists" refilling emptied niche space.

Our purpose is to quantify trends, periodicities, events, and self-organization from the evolutionary record by using advanced methods of time-series analysis, such as wavelet analysis (i.e., Grossman and Morlet 1984). We also correlate the PF record statistically and graphically with other geological records. We use the most recent time scale available (Gradstein and Ogg 1996) and consider both gradualist and catastrophic models used to explain evolutionary pattern. The PF record was chosen for the study, because it provides more detailed biostratigraphic resolution than any other group (Berggren and Casey 1983; Patterson and Fowler 1996). A data-driven nonlinear model with parameters consistent with the results of the wavelet analyses is constructed. The model demonstrates that an interplay of external and self-organized factors is feasible to explain the dynamics underlying the long-term evolution of planktic foraminifera.

It is not our aim to investigate and discuss the specific consequences of environmental parameters on evolution of morphotypes, phylogenetic linages, nor short-time (≤2 Ma) patterns in the PF-evolutionary record. For details in these areas of study, we referred to the research of Brasier (1988), Hart (1990), Banerjee and Boyajian (1997), and Pearson (1998).

Paleontological and geological data

Planktic foraminiferal taxonomy is continually being improved, because planktic foraminifera are stratigraphically important and abundant in small samples of most marine sediments. The wide paleogeographic distribution of PF reduces the possibility of artificial extinction–origination levels, the "Signor–Lipps-effects" (Signor and Lipps 1982) and the evolutionary influence of geographical barriers. To construct the database, descriptions of 1654 species were utilized; subspecies and variants provided by Ellis and Messina (1940 and yearly supplements) were also examined. In addition, the stratigraphic and paleoceanographic literature of PF were consulted (Kennett and Srinivasan 1983; Bolli et al. 1989; Hart 1990; MacLeod and Keller 1994). Patterson and Fowler (1996) used only genuine species and rejected synonyms, subspecies, and intraspecies variants, as well as poorly documented forms and taxa with indeterminable stratigraphy. Patterson and Fowler's (1996) database consisted of 662 species over 217 stratigraphic levels. Some taxa thought to be survivors of the K–T boundary event are now known to be reworked forms from the Cretaceous (Kaiho and Lamolda 1998) and are removed from the database. Additionally, a new compilation of Paleocene to Oligocene PF by Pearson (1998) is now included in our study. For this study, 622 reliable species form the complete database, from 200 stratigraphic levels from Barremian to recent. The complete data used for this study are available from << http://www.carleton.ca/~tpatters >>.

Relative extinction is calculated by division of number of species that became extinct during a stratigraphic interval with the number of species, which occurred at the previous level. Relative origination is calculated in a similar manner. All stratigraphic levels were calibrated to the time scale of Gradstein and Ogg (1996). This time scale is constructed using the most advanced techniques, including statistical, geochronological, and graphical procedures (Agterberg 1994), and has a mean standard error of ~0.5 Ma per stage boundary.

Two sets of time series from the PF record were constructed that represent (*a*) dominance of gradual increase or decrease in PF diversity, and (*b*) discrete (abrupt) events in the decrease and increase of PF diversity from one to the next stratigraphic level, respectively. The first set contains extinctions or originations that are calculated using a moving average, with a window width of 1 Ma and stepwise movement of the sliding window in 1 Ma increments. In this way, we assume that the stratigraphic levels (e.g., subzone boundaries) used may mark cumulation of extinctions and radiations, which originally happened between subzone boundaries. For discrete sets (better described as "event" sets), it is assumed that radiation and extinction may have happened over short-time intervals at zone or subzone boundaries. We set the duration per event at 40 ka, corresponding to the well-dated duration of the extinction processes of the *Rotaliporidae* in the late Cenomanian (Luderer and Kuhnt 1997).

Average data for equally spaced 1 Ma intervals of all data sets were used to permit linear correlation, autocorrelation, spectral analysis, and cross-spectral analysis. In this way, the time resolution of some geological events is reduced, but the influence of possible errors in the time scale of about ±0.5 Ma is also reduced. Additionally, a data set "change in the total number of species per 1 Ma" gives the balance of total extinct and originated PF species number, and therefore a measurement of persistence in the PF evolution.

Time-series analysis

Spectral analysis, linear correlation, autocorrelation, and cross-spectral analysis are common statistical tools for

time-series analysis of geological data (e.g., Davis 1986; Schwarzacher 1993; Fischer and Koerner 1994), while wavelet analysis is relatively new for geological time-series analysis (Bolton et al. 1995; Prokoph and Barthelmes 1996). Spectral analyses transform the signal from time to frequency domain. Significance tests are also well established (e.g., Davis 1986). We used the "red noise" and "white noise" definition after Bartlett (1966) and the calculation method demonstrated by Mann and Lees (1996) to determine the significance of periodicities detectable by Fast Fourier transform (FFT). However, spectral analysis (e.g., FFT) has the serious drawback that time information is lost.

In contrast, wavelet analysis permits distinction between stationary and nonstationary signals, such as gradual and abrupt changes in signal frequency, phase, and amplitude. The wavelet transform of a time series is defined as

$$[1] \qquad W\psi\ (a, b) = \left(\frac{1}{\sqrt{a}}\right)\int f(t)\psi\left(\frac{t-b}{a}\right)dt$$

where ψ is the base wavelet, with a length that is usually much shorter than the time series *f(t);* the variable *a* is the scale factor that determines the characteristic frequency, so that varying *a* gives rise to a spectrum, and *b* is the translation in time so that varying *b* represents the "sliding window" of the wavelet over *f(t)* (Chao and Naito 1995). Thus, the wavelet transform uses narrow windows at high frequencies and wide windows at low frequencies. The graphic representation of the wavelet coefficients in the time–frequency space is a "scalogram" (Fig. 1).

We have utilized a continuous wavelet transform (CWT), with the Morlet wavelet as mother function (Grossman and Morlet 1984). The shape of the Morlet wavelet is similar to a periodic sinusoidal function, which is suitable for detection of cycles with unknown geometrical shape. To enable an arbitrary shift of the wavelet transform resolution in favor of time or in favor of frequency, a parameter *l* is introduced representative of the length of the mother wavelet (Prokoph and Barthelmes 1996). Low values *l* support better solution of time-domain (i.e., detection of discontinuities and other singularities), and high value *l* support a better resolution in scale (wavelength). Thus, the shifted version of the Morlet mother wavelet used is defined as

$$[2] \qquad \psi^{l}_{a,b}(t) = \pi^{-\frac{1}{4}}(al)^{-\frac{1}{2}}\, e^{-i2\pi\frac{1}{a}(t-b)}\, e^{-\frac{1}{2}\left(\frac{t-b}{al}\right)^2}$$

In this work, a value $l = 10$ was chosen, because it gives results that are satisfactory in both time and frequency (Prokoph and Barthelmes 1996). To transform a measured, and hence limited and discrete time series, the integral in eq. [1] has to be modified by using the trapezoidal rule for unevenly sampled points to evaluate the wavelet coefficients giving $W^*_l(a,b)$. Therefore, the method does not require series consisting of equally spaced data intervals, as the other time-series analysis methods used. The data were standardized around a mean = 0, and overlying trend ("fitting line") was removed before performing the wavelet transform. The visualizing of $W^*_l(a,b)$ has been carried out by interpolation and coding with appropriate shades of gray. In our approach, we used four gray levels of the magnitude of the wavelet coefficients in the graphic presentations, with black representing 75–100%, dark gray 50–75%, light gray 25–50%, and white 0–25% of maximum $W^*_l(a,b)$.

A wavelet transform of a computer-generated time-series model using the above analysis conditions is shown in Fig. 1. Nonstationary, high-frequency wavelet coefficients appear in time intervals dominated by random white noise. Unique events (singularities) form high wavelet coefficients for short time at high frequency. Stationary and nonstationary periodic signals form continuous and discontinuous narrow bands of high wavelet coefficients, respectively. In contrast, Fourier transform cannot distinguish nonstationary from stationary signals and gives a nonstationary periodic signal a reduced power comparable to white noise (Fig. 1*c*). Consequently, confidence tests as used for stationary signals (e.g., Davis 1986) are not feasible for evaluation of nonstationary signals and are not used in this study.

Wavelet-analyses methods, computer program CWTA.F, and parameters used are described in Prokoph and Barthelmes (1996). For time-series analysis of the paleontological and geological data, only periods longer than 2 Ma were analyzed, because of resolution limits due to the Nyquist frequency $f_N = 2^*\Delta t$ (Davis 1986).

Periodicity and self-organization in the PF record

Wavelet analysis of the total number of PF species shows a conspicuous black band in the wavelet scalogram representing a quasi-stationary 31–32 Ma periodicity (Fig. 2*a*). Additionally, a weak secular trend forming a 95 Ma periodicity (dark gray areas in Fig. 2*a*) is apparent. A 14 Ma periodicity occurs since the Eocene. Periods of 3.8 and 10 Ma correspond to the sharp reduction in PF species numbers at the K–T boundary and during the Oligocene.

Wavelet scalograms of the "event" set (Fig. 3*a*) and "gradual change" data set (Fig. 3*b*) reveal a ~28 Ma and ~30 Ma quasi-stationary periodicity of relative PF-origination data, respectively. In both data sets, nonstationary 13 and 4.5 Ma periods occur from Campanian to Oligocene, and 8 Ma periods from Barremian through Albian. The relative PF-extinction data show well-pronounced stationary ~29–30 Ma periodicity in both "event" (Fig. 3*e*) and "gradual change" data sets (Fig. 3*f*) and nonstationary ~10 Ma periodicity from Turonian through Eocene. A punctuated 2.5–3.2 Ma periodicity appears from late Maastrichtian through Paleocene, forming approximately five cycles in the relative PF-extinction record. Additionally, a ~80 Ma periodicity appears in wavelet scalogram of the event set of both relative PF-origination and -extinction data. A secular trend of ~100 Ma periodicity is interpreted from the contrast of high origination and extinction rates around 60–65 Ma and relatively low origination rates before 95 Ma and after 35 Ma (Figs. 3*c*, 3*d*). This 100 Ma wavelength may coincide with a periodicity detected in the much longer Phanerozoic seawater isotope record of carbonate rocks (Prokoph and Veizer 1999).

The extraordinary high relative PF extinction at 65 Ma (K–T boundary) of 97.7% and successive recovery in early Paleocene form events in the data sets comparable to the singularity illustrated in Fig. 1. Spectral analysis (FFT) indicates a dominant period of ~31 Ma for relative PF-extinction

Fig. 1. (*a*) Wavelet analysis of computer time-series model. Top: intensity scale of wavelet coefficients in four gray levels; middle: wavelet scalogram shows the vertical axis with logarithmic-scaled time period, horizontal axis is time; bottom: model data with random ("white") noise from 0 to 50 t.u. and amplitude of 1; singular event at 65 t.u. with amplitude of 0.9; stationary 30 t.u. sinusoidal period with amplitude of 0.2; and nonstationary 10 t.u. sinusoidal period with amplitude of 0.2 from 20–45 t.u. and 80–110 t.u. (*b*) Computer time-series model with 1320 equidistant data forming 132 time units (t.u.). (*c*) Fourier transform of the computer time-series model. Note that all major signals are captured in the wavelet analysis, but that the nonstationary 10 t.u. period is hardly distinguishing from background (white) noise.

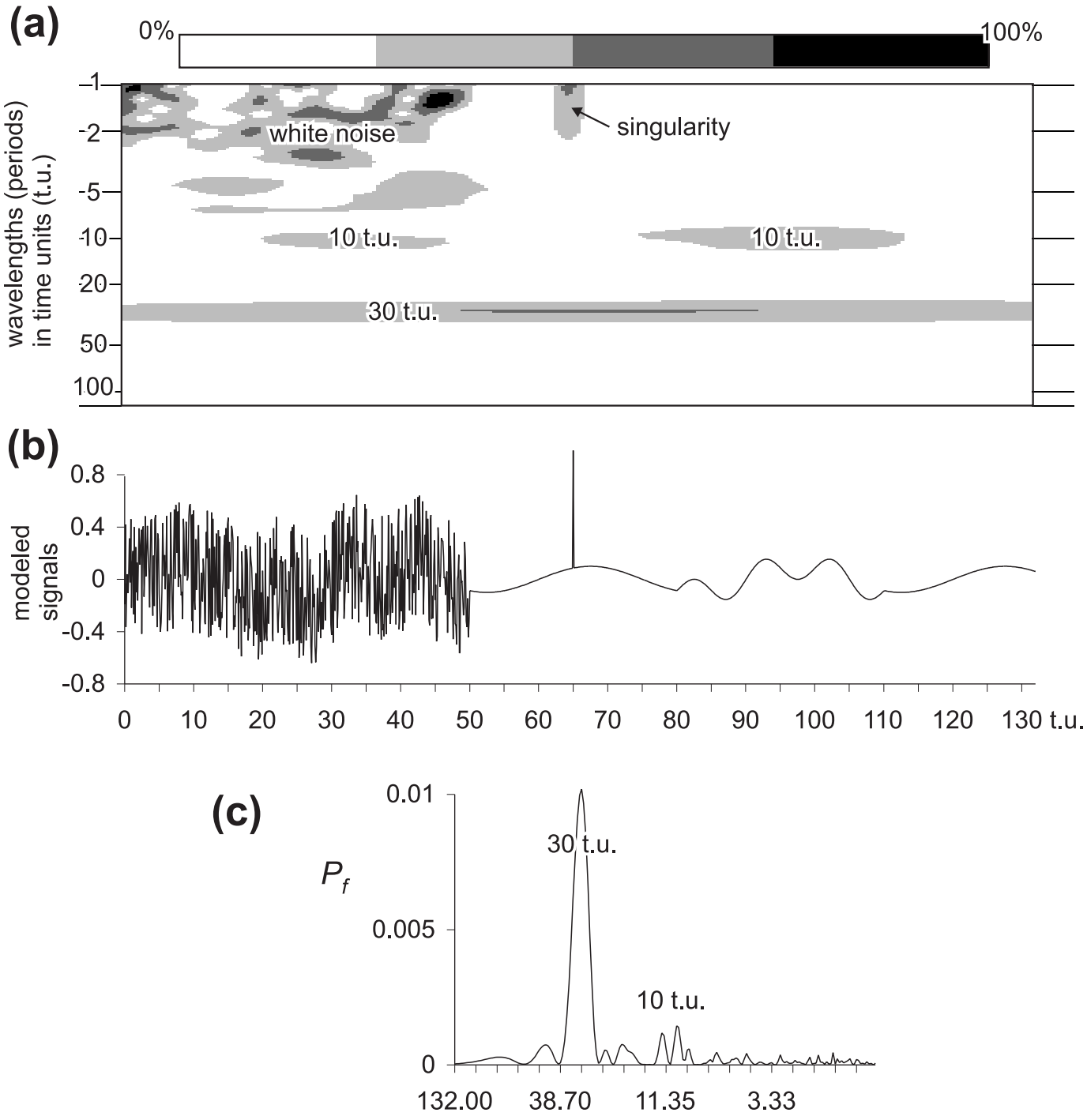

data with and without use of the extreme values at the K–T boundary (Fig. 4). The 3.2 Ma period is strong in FFT (Fig. 4), but shown to be nonstationary in wavelet analysis (Fig. 3). The 10 Ma extinction periodicity is only evident with the K–T boundary extrema (Fig. 4*a*) and is also nonstationary (Fig. 3). Long periodicity >60 Ma cannot be resolved in small bandwidths with FFT. The red noise level is low for relative PF extinction, origination, and changes of number of PF species /1 Ma as shown by the low lag-one autocorrelation coefficients (i.e., AR(1)) in Table 1.

Fig. 2. Wavelet analysis of a number of planktic foraminifera (PF) species in the last 127 Ma. (*a*) scalogram with intensity scale for wavelet coefficients and axis as in Fig 1; Ages of major periods are marked in scalogram. (*b*) Species data, for data compilation see text; time scale after Gradstein and Ogg (1996); vertical stripped line shows K–T boundary.

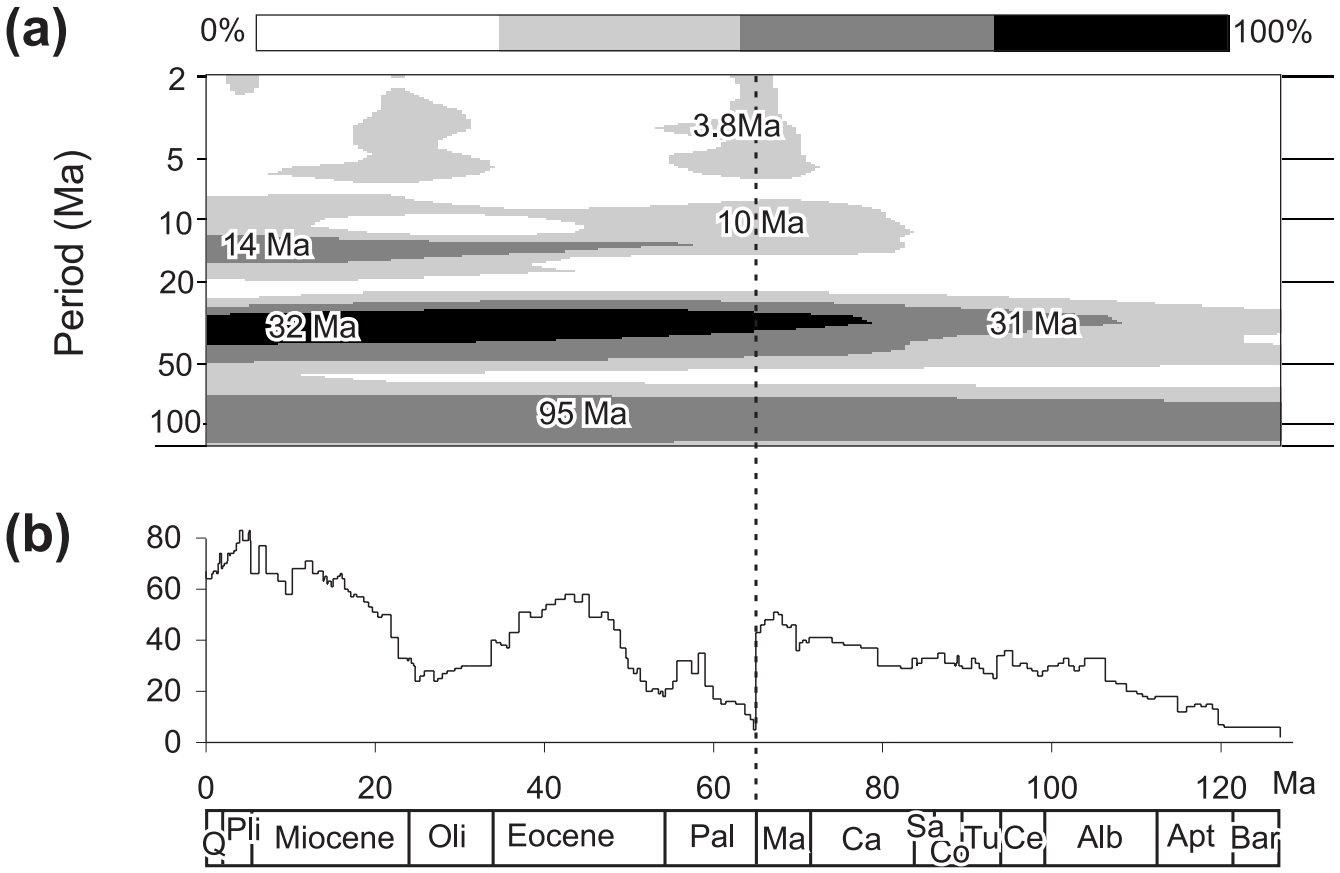

The PF pattern appears to have two types of evolutionary response to disturbances, which can be interpreted as persistence and resilience, according to the terminology of Miller (1996). Resilience, that is, the recovery to an initial state following a disturbance, appears in PF data, for instance, after the K–T boundary, where a high origination event occurs after about 0.1 Ma. The correlation between PF extinction and origination is significant with $r = 0.38$, which increases to $r = 0.43$ without consideration of the K–T extrema (Table 1). The approximate stability of baseline number of PF species after extinction and origination events marks persistence. Extinct species are replaced quickly and often by species with similar morphotypes (Hart 1990). This behavior can be attributed to self-organization of nonlinear chaotic systems, in that (1) the changes of the PF extinction through time are bounded within a range of values (Patterson and Fowler 1996), a so-called attractor, and that (2) power spectrum, based on a 2 Ma resolution of the PF-extinction record, follows a superimposed 1/*f*-trend of the power-law relationship (Sole et al. 1997; Newman and Sibani 1999).

Models

Our model for long-term evolution of planktic foraminifera is based on the kinetic response to a system with an oscillatory input

$$[3] \quad dM/dt = b + a\sin(\omega t) - kM$$

as described by Lasaga (1998), where a is the average input rate (e.g., sea-level change), k is a first-order constant, and M can be interpreted as the amount of PF species at a distinct time. Such an oscillatory system model gives the conceptual model for possible external-forced self-organization of biological systems, such as planktic foraminiferal evolution (Fig. 5).

From studies of biological evolutionary processes, a nonlinear component providing self-organized patterns is shown to be very likely involved in their dynamics (Bak and Sneppen 1993). Our data-driven model makes use of the logistic map representing the simplest of all nonlinear equations. Recall that in the differential equation of growth (May 1976),

$$[4] \quad \delta x/\delta t = \lambda x$$

growth of units x with time t varies as a function of the amount of x scaled by a growth constant λ. Substitution of values into these solutions, when $\lambda > 0$, results in unbounded exponential growth. Clearly this is not a physically real situation, as all systems must eventually peak, plateau, or die out. However, growth can be bounded simply by scaling eq. [4], as follows

$$[5] \quad \delta x/\delta t = \lambda x(1 - x)$$

i.e., the logistic equation. Although the analytical solution to this equation is rather uninteresting, the finite difference form

$$[6] \qquad x_{t+1} = \lambda x_t\ (1 - x_t)$$

termed the logistic map, has extremely rich behaviour and has been extensively studied (Feigenbaum 1978) and used as a simple analogue of biological populations (May 1976).

Time series of the logistic map are attained by iterating eq. [6], with seed values of n [0,1] for different values of the "control parameter" λ [0,4]. For values of λ [1,3] output series are regular in nature and characterized by convergence to single values. With increasing λ, period-doubling bifurcations having multiple values of x occur, until $\lambda > 3.57$, where "chaotic regions" with infinite though-bound unstable values for x begin (May 1976).

To illustrate the type of possible dynamical regime for the PF evolution, we construct a data-driven self-organization (SO) model based on the logistic map and the following parameters for external forcing:

(1) A 30 Ma periodic component as determined by our wavelet analysis of the PF record is used. An average phase shift of $s = 5$ Ma is determined from the age of extrema e_i, the relative PF extinction at about 34–36 Ma ($i = 1$), 65 Ma ($i = 2$), and 93.5 Ma ($i = 3$) by

$$s = e_i - (i\ *30\text{Ma}).$$

(2) A weak 100 Ma periodicity is also included resulting from the weak secular trend in PF record (Fig. 3), with a phase shift of 20 Ma due to high extinction rates around Maastrichtian – early Paleocene and relatively low PF extinction rates before 97 Ma and after 33 Ma.

Consequently, we used for our model an amplitude of 0.2 for the 100 Ma periodicity with –20 Ma-phase shift and an amplitude of 0.8 for the 30 Ma periodicity with –5 Ma phase shift. All nonstationary periods detected in the PF record are not included in our model. Because the approximate standard error of the time-scale calibration is ± 0.5 Ma (Agterberg 1994), we used for our Model $\Delta t = 1$ Ma. Thus, the modeled values represent intervals; for example, 126.5 Ma represents 126–127 Ma. The periodic forcing parameter ϕ (corresponding to say, bolides or volcanic episodes) oscillates in time, t,with Δt in Ma within the ϕ range [0, 2] as

$$[7] \qquad \phi_t = 0.8\left(1 + \cos\left(\frac{2\pi t - 5}{30\Delta t}\right)\right) + 0.2\left(1 - \cos\left(\frac{2\pi t - 20}{100\Delta t}\right)\right)$$

We chose λ ranging from [3, 4] compatible with evolution being at the "edge of chaos," as postulated by Kauffman (1993). The value of λ is determined by substitution

$$[8] \qquad \Delta x/\Delta t \rightarrow x_{t+1} = (3 + \phi_t/2)\ x_t\ (1 - x_t)$$

Realizations of eq. [8] depict relative extinction (x below average) and relative origination (above average). For comparison, we applied an alternative model based on a periodic driven white noise function. Other noise types with "time-memory" (e.g., autoregressive noise, random walk) are not considered, because of the low AR(1) autocorrelation of the data studied (Table 1, Fig. 4). The white noise amplitudes "F_t" of our alternative NOISE model are adjusted to the same amplitudes as the SO model.

$$[9] \qquad x_t = -0.5F_t\ a\sin(\omega t) + 1$$

For this model, we substitute $a\sin(\omega t)$ for eq. [7] to obtain our 'NOISE PF-model':

$$[10] \qquad x_t = -0.5\mathrm{F}_t\ \phi_t + 1$$

Models versus data

Fig 6 shows a realization of the SO Model with initial value of $x_0 = 0.3$ at 128 Ma. This simulation corresponds exactly with the high relative PF extinction at the K–T boundary (65.5 ± 0.5 Ma), as a result of the 30 Ma periodic forcing. Moreover, some modeled extinction events (negative extrema) correlate well with the actual relative PF-extinction data ($r = -0.305$), as a result of underlying logistic map (dashed lines in Fig. 6). Corresponding intervals (±0.5 Ma precision) are at 6.5, 10.5, 33.5, 37.5, 57.5., 60.5, 64.5, 93.5, and 101.5 Ma. Furthermore, eight of the 11 major negative peaks in the SO model correlate with eight of the 18 highest relative PF extinction rates, which is a significant correlation ($r = 0.44$). In contrast, variation in relative PF origination is less well explained by the SO model. Major extinction events of our SO model are phase shifted to the periodic forcing function (e.g., 93.5 Ma instead of 95.5 Ma) as shown in Fig. 7. The 100 Ma periodic forcing is truncated to an ~85 Ma period. These alterations in periodicity and phase are results of the nonlinearity in the SO model. However, similarities of 80–85 Ma period found in the PF-extinction and -origination data (Fig.3), as well as the correspondence of phase-shifted minima in the SO model with PF-extinction events are striking.

In contrast, distinct abrupt extreme values in the NOISE models correspond only with extinction events at the K–T boundary and high relative PF origination in early Aptian, middle Paleocene, and early Miocene (Figs. 6*c*, 6*d*). The NOISE model does not correlate with extrema in PF extinction ($r = -0.03$) and origination ($r = -0.12$).

The periodicities of the SO model of 2.45 and 4.5 Ma for the Paleocene (Fig. 6*a*) and the ~30 Ma period appear 3.14 radians (about 180 degree) phase shifted to the relative PF-extinction data (Fig. 7), which means that they correspond well with the realizations from eq. [8] of the SO model (extinction events related to minima in the model).

Nonstationary 15 Ma to 2.5 Ma periodicities appear in the SO Model, but also in the NOISE model. Similarities to our PF record makes it likely that multiple periodicity of less than 10 Ma is forced by a low-dimensional internal self-organization or randomly by multiple independent causes. However, the stratigraphic resolution and the uncertainty in the identification of PF species limit a quantitative interpretation of magnitude and high-frequency periodicity involved in the PF evolution.

Discussion

Periodicity

The major ~30 Ma periodicity in the PF record is similar to the 27 Ma periodicity found in the PF origination (Hart 1990)

Fig. 3. Wavelet analysis of relative PF origination and extinction in the last 127 Ma; for explanation of scalogram see Fig. 1. (*a–c*) Analysis of relative PF origination: (*a*) scalogram from data considered as punctuated events, (*b*) scalogram from data considered as gradual changes, (*c*) data at event levels with 20 Ma moving-average curve (dashed line). (*d–e*) Analysis of relative PF-extinction data: (*d*) data at event levels with 20 Ma moving-average curve (dashed line), (*e*) scalogram from data considered as punctuated events. (*f*) Scalogram from data considered as gradual changes; dashed line shows K–T boundary.

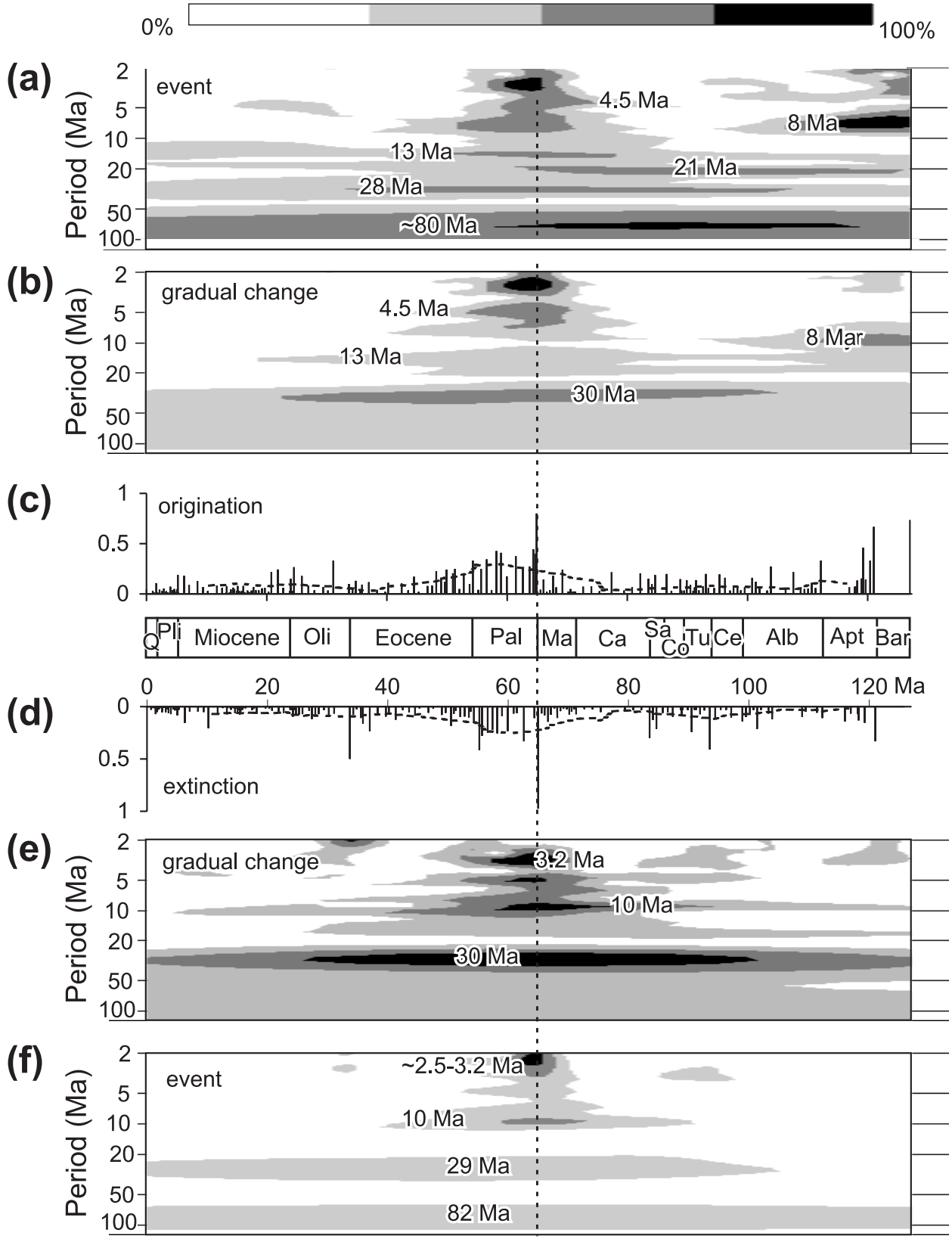

Table 1. Matrix of linear-correlation coefficients for 127 data (Δt = 1Ma).

		AR(1)	1	2	3	4	5	6	7	8	9
1	Δ no. PF species/1Ma	0.11	—	**–0.49**	–0.35	0.19	0.13	0.03	–0.14	–0.10	0.16
2	Relative PF extinction	0.23	**–0.49**	—	**0.42**	0.38	–0.23	–0.05	–0.02	**0.69**	0.26
3	Σ impact diameter	0.03	**–0.35**	0.42	—	0.02	–0.06	–0.04	0.09	–0.09	–0.03
4	Relative PF origination	0.13	0.19	**0.38**	0.02	—	–0.09	0.02	**–0.21**	0.04	**0.64**
5	Detrended sea level	0.73	0.13	**–0.23**	–0.06	–0.09	—	**0.39**	0.14	–0.16	–0.01
6	Sea level	0.96	0.03	–0.05	–0.04	0.02	**0.39**	—	**–0.57**	–0.07	–0.01
7	Number PF species	0.96	–0.14	–0.02	0.09	**–0.21**	0.14	**–0.57**	—	0.00	–0.10
8	Relative PF extinction (a)	0.13	–0.10	**0.69**	–0.09	0.04	–0.16	–0.07	0.00	—	**0.43**
9	Relative PF origination (a)	0.24	0.16	**0.26**	–0.03	**0.64**	–0.01	–0.01	–0.10	**0.43**	—

Note: Bold numbers indicate correlation >95% confidence level at $|r| > 0.19$; (a), without K–T-boundary extrema; AR(1), lag-one autocorrelation coefficient.

Fig. 4. Spectral analysis (Fast Fourier Transform) of relative PF extinction (*a*) including and (*b*) without extreme high values at the K–T event at 65 Ma. Long-dashed lines mark red noise level; short-dashed lines mark white noise variance. Marked periods of 31, 10, and 3.2 Ma are above a spectral power of 0.1.

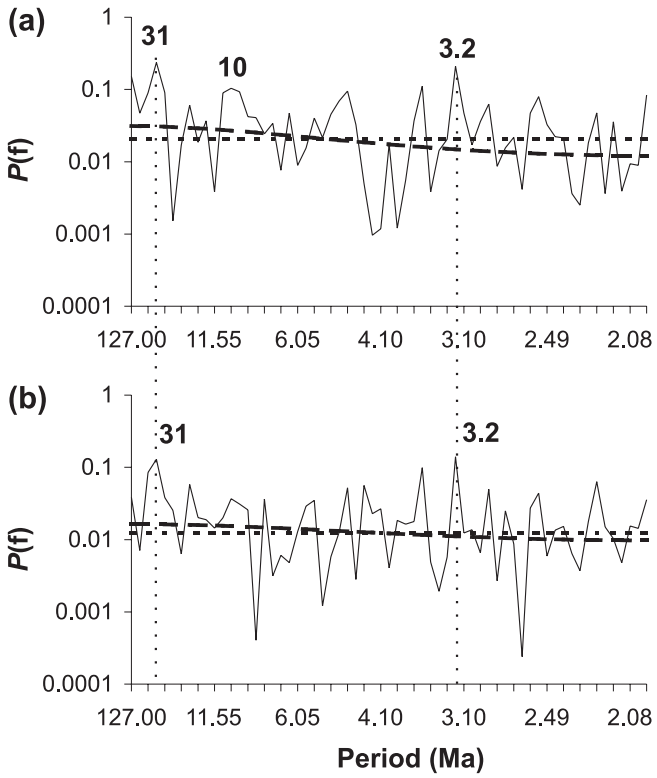

and to the 26–30 Ma periodicity in the mass-extinction record of the last 250 Ma (e.g., Raup and Sepkoski 1984; Rampino and Stothers 1984). The PF-extinction record shows better pronounced long-term periodicity (i.e., ~30 and 85 Ma) and clearer patterns of self-organization than the PF-origination record. The PF-origination record appears statistically more random, as already shown by nonlinear analysis techniques by Patterson and Fowler (1996).

The existence of a 26–30 Ma periodicity in the fossil record has been critically debated for more than a decade, especially because of the

(1) limited quality of the time scales, the dating of stratigraphic boundaries used, and the possible insignificance of periodicity (e.g., Hoffman 1985, 1989; Stigler and Wagner 1988),

(2) the insufficient quality of the database (marine taxa, culled data, preservational constraints) and the taxonomic level (family, genera, species) used (Patterson and Smith 1987; Benton 1995),

(3) the statistical methods used (e.g., FFT) may have favored the detection of periodicities that are multiples of the mean durations of stages (Stigler and Wagner 1988 vs. Raup and Sepkoski 1988).

However, statistical tests have demonstrated that the 26 Ma periodicity cannot be an artifact of variances in spacing of the peaks in the mass-extinction database (Kitchell and Estabrook 1986). Also, the data base has improved over the last decade (Sepkoski 1998). Our PF database has 200 extinction–origination levels over the last 127 Ma and provides a much more detailed record than mass-extinction studies with 24 stage boundaries used from Recent to the Barremian (Raup and Sepkoski 1986; Rampino and Caldeira 1992). The time scales are also greatly improved (i.e., Gradstein and Ogg 1996) by more accurate and precise radiometric dates (e.g., Obradovitch 1993) and correlation techniques (Agterberg 1994). There is still the problem that some stages are very long (e.g., Aptian, Albian, Campanian), and the time resolution within the stages is relatively poor. This inaccurracy in the time scale can lead in particular to imprecise periodicities at high frequencies (low wavelengths) in the fossil record, something we do not evaluate in this study.

The ~30 Ma periodicity in the PF-evolutionary record presented here is slightly longer than the mass-extinction periodicity of 26–30 Ma proposed previously, because

(1) different time scales were used. Mass-extinction levels move from 91 to 94 Ma for the late Cenomanian and from 36.6 to 33.7 Ma for the late Priabonian, using the time scales of Palmer (1983) and Gradstein and Ogg (1996), respectively;

(2) the high PF-extinction rate in late Miocene at ~ 6.5Ma is not a mass-extinction level, possibly because of particularly limiting environmental conditions for PF (e.g., competition or restricted food resources, oceanic circulation disturbances).

(3) the wavelet transform permits a better time–frequency resolution than the Fourier transform (Fig.1), This is also demonstrated by the fact that the wavelet scalograms are identical in terms of their long-term cyclicity, when considering either the gradual or event data (Fig. 3).

Fig. 5. Conceptual model for periodic forcing of self-organized evolution and schematic PF extinction–origination pattern, modified after Lasaga (1998).

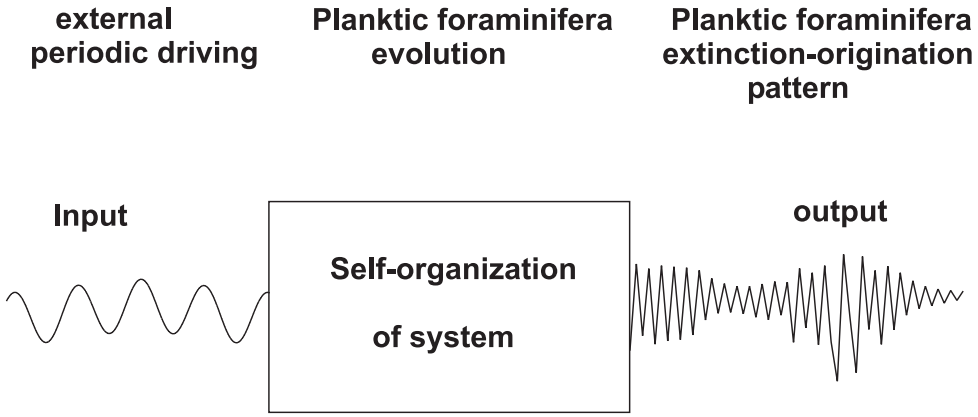

Model

The SO model provides an explanation for high-frequency periodicities, singularities, extreme events, which are phase shifted to the overlying long periodicities, and resilience episodes in the PF record, through the use of a low-dimensional dynamic system (i.e., two periodic and a nonlinear parameter) and without invoking multiple external causes. Our results support the idea that external perturbations, such as 30 Ma and 100 Ma cycles, enhance self-organized evolution (e.g., Plotnick and McKinney 1993), or alternatively that nonlinear evolutionary changes may occur that are dependent on the intensity of physical disturbances (Chiba 1998). Other models that include significant random noise due to errors in the PF record and the time scale or that exclude or include more periodic forcing functions are possible. It is also possible to model extinction and origination dynamics separately (Newman and Sibani 1999), respect faunal provences, and more importantly respect biological processes instead of the fossil record itself (e.g., Plotnick and McKinney 1993; Huismann and Weissing 1999), which make the output more accurate, but also much more complicated.

Our model cannot express the variability in the time intervals between extinction and origination events nor the absolute number of PF species possible in the environment. Both time intervals and total PF-diversity estimation are subjects to various measurement errors that reduce the feasibility of more distinct data-driven modelling at this stage. The comparison of the SO model and NOISE model leaves the question open whether the high-frequency periodicity is predominantly a nonlinear effect (Fig. 6*a*) or more random (Fig. 6*e*). However, the NOISE model provides neither phase shifts of the periodic forcing function nor extreme values as the K–T boundary extinction event. Sole et al. (1997) showed that the temporal distribution of relative PF extinction resembles a power law distribution, which is characteristic of self-organization.

Correlation with geological events and changes

Impact crater record

The terrestrial impact crater record (Fig. 8) is linearly correlative to relative PF extinction and to the changes of number of PF species/Ma (Table 1). Also, the pattern of nonstationary ~2.5–14 Ma periods and the quasistationary ~30 Ma periodicity in the wavelet analysis of the impact record (Fig. 9*a*) correspond to the periodicity in the relative PF extinction (Figs. 3*d*–3*f*). However, the 30 Ma periodicity of the PF extinction data is phase shifted by 2.57 radians, which corresponds to ~6.5 Ma = 31 million years*1.31/2π to the terrestrial impacts (Fig. 10). Moreover, linear correlation between the terrestrial impact crater record and relative PF extinction is not significant once the K–T extinction event is removed and replaced by a value of zero (Table 1). Therefore, a significant correlation between Phanerozoic mass extinctions and impact cratering (e.g., Rampino and Stothers 1986; Sepkoski 1989; Matsumoto and Kubotani 1996) is not evident for the PF evolution. However, these studies did not take the sizes of all impact craters and the errors of the time scale into consideration, which are both changed due to newer data. Nevertheless, correlations exist between the K–T-boundary impact, the Popigai and Chesapeake crater ages, and the PF evolutionary record (Fig. 8) and in the 10 Ma periodicity around the K–T boundary (Fig. 10).

Glikson (1999) has calculated that approximately 10 craters (3 on the continents and 7 in the ocean basins) greater than 100km in diameter should have collided with Earth over the past 127 Ma, although there is only evidence, thus far, of three on the continent: Chicxulub (170 km at 64.98 ± 0.05 Ma, Chesapeake(90 km at 35.2 ± 0.3 Ma), and Popigai (100 km at 35.7 ± 0.8 Ma) (Grieve 1997; R.A.F. Grieve, personal communication, 1999). Iridium anomalies (e.g., Alvarez et al. 1982; Asaro et al. 1982) may indicate a bolide impact linked to the increased PF-extinction rate around the Eocene–Oligocene boundary. Thus, the Popigai and Chesapeake craters and other undiscovered bolide impacts cannot be rejected as potential causes of PF-extinction events. A significant correlation between mass-extinction and impact crater ages found by Matsumoto and Kubotani (1996) was suggested as insignificant after removing of the impacts >40 km from the data set (Yabushita 1998). Consequently, we assume that smaller PF-extinction events and small impacts with craters <40 km diameter are unrelated.

Sea level

Sea-level fluctuations are assumed to be major causes for mass extinction (i.e., Hallam 1989) and fluctuations in the

Fig 6. (*a*) Scalogram of wavelet analysis of (*b*) a coupled, periodic, nonlinear model (SO Model) with Δt = 1 Ma of 127 Ma; for comparison: (*c*) relative PF origination (above zero) – extinction (below zero), (*d*) periodic, forced, random noise (NOISE) model with Δt = 1 Ma; (*e*) wavelet scalogram of NOISE model. Vertical dotted lines in (*b*) and (*c*) mark correlations between SO model and relative PF extinction; bold dashed line marks K–T-boundary event in PF data and SO Model; horizontal dashed lines in (*b*) and (*d*) mark mean, indicating assumed transition between modeled extinction level (below line) and origination level (above line); asterisks in (*d*) mark negative extrema in NOISE model, in phase with periodic forcing function; for further explanation see text.

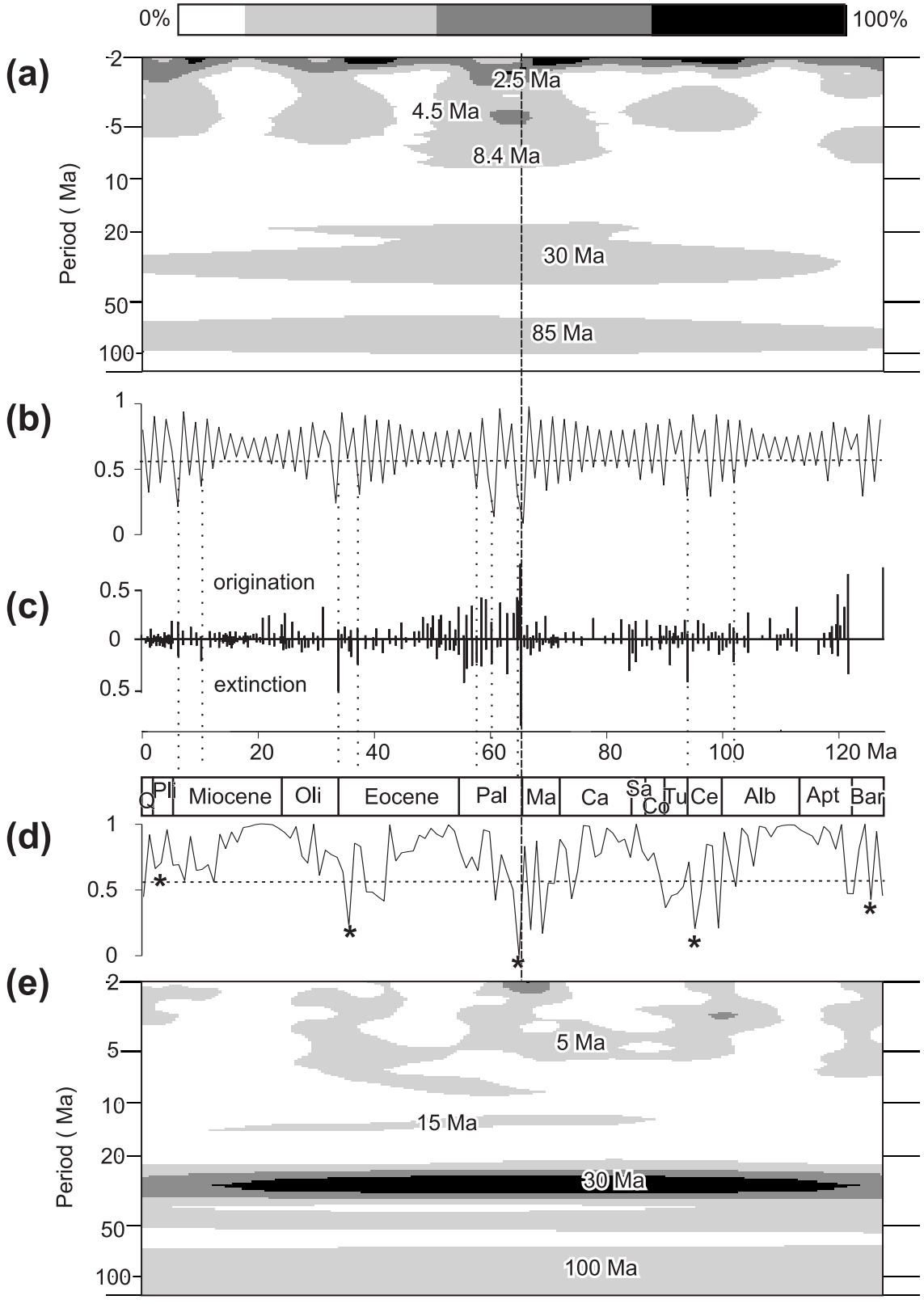

Fig. 7. Cross-spectral analyses of relative PF-extinction data with SO model data. (*a*) Cross-amplitude, (*b*) phase spectra. Δt = 1 Ma. Vertical lines mark correlative or negative correlated (180 degree phase shifted) peaks.

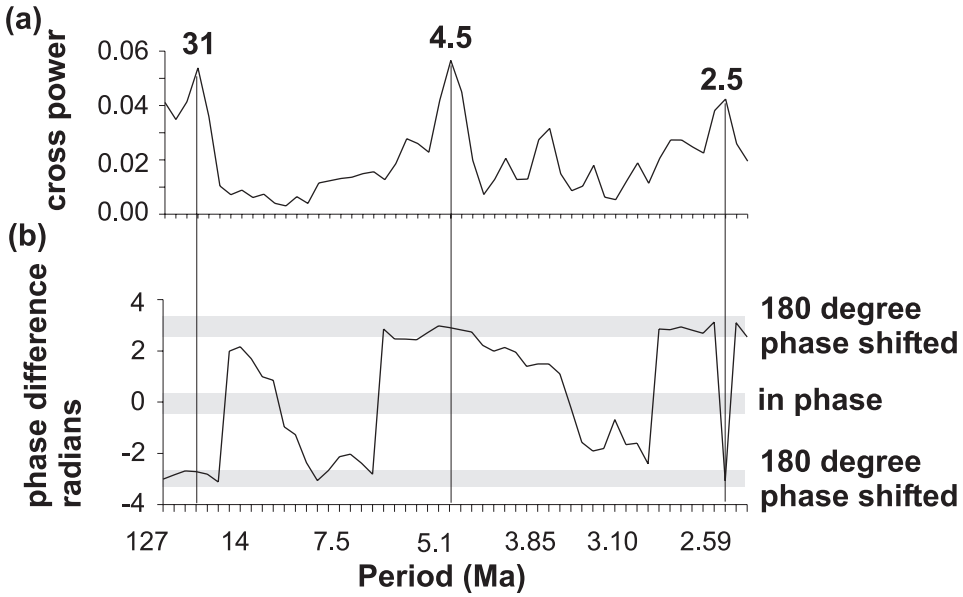

origination of PF species (Hart 1980, 1990). Wavelet analysis reveals an approximate 27.5 Ma periodicity in the sea-level changes, but it is superimposed by other nonstationary 3.8, 8, 16.5, and 42 Ma periods (Figs. 9*c*, 9*d*). Cross-spectral analysis shows that there is a phase shift between the 27.5 Ma periodicity in sea level and the ~30 Ma periodicity in the PF record of 2.57 radians, which corresponds to 10.6 Ma = 26*2.57/2π or inverserly corresponds to low sea level at high extinction rates, 2.3 Ma = 26*(π –2.57)/2π (Fig. 10). Despite the phase shift, a weak though significant linear correlation (r = –0.23, Tab. 1) exists between PF extinction and sea-level change. For instance, severe global sea-level falls in the late Turonian (90.5 Ma), late Paleocene (58.2, 55.2 Ma), and late Eocene (37, 33.7 Ma) correspond with increased PF-extinction rates >0.2 (Fig. 8). This obvious correspondence may be statistically random, because only three of the major eight sea-level drops have a correlation to the PF-extinction rate. The high correlation (r = –0.57) between total number of PF species and sea level is also insignificant, because of the strong time-dependence (AR(1) > 0.9) of both data sets (Table 1).

Consequently, periodicities in sea-level change and impact record are not significantly linked to relative PF extinction, but correspondences of some large impacts and sea level-falls exist with the PF record. New recalibrations of the time scale and extended and improved impact age determinations may change the significance of any possible relationships.

Flood-basalt epochs, oceanic anoxia, and increased $\delta^{13}C$ levels

Correlations made by inspection, due to the sparseness of data, support a relationship between two oceanic plateau basalts, five of seven continental flood basalts, and two of three anoxic events with the ~30 Ma periodicity in PF evolution (Fig. 8). For instance, an oceanic anoxic event coincides with the extinction of the *Rotaliporidae* at the Cenomanian–Turonian boundary (e.g., Brasier 1988). In particular, a 26–32 Ma periodicity in the flood-basalt volcanism from a 250 Ma record (Rampino and Stothers 1988; Yabushita 1998) has the same periodicity as the PF record. Additionally, a significant positive $\delta^{13}C_{Carb}$ peak of about 3‰ (Veizer et al. 1999) corresponds with relative high PF extinction in the late Paleocene.

Causes and consequences

From the above correlations, we can postulate two general causes that increased PF-extinction and radiation rates: (1) Mantle degassing as the result of flood-basalt volcanism increased the atmospheric CO_2 level, released a large mass of sulphur-rich gases in the stratosphere–troposhere, and disturbed the oceanic circulation pattern and ocean chemistry. This degassing increased the carbon input in the oceans and provided thicker oxygen minimum zones, triggering oceanic anoxic events (e.g., Schlanger and Jenkins 1976; Kerr 1998). Loper et al. (1988) modeled a cyclic instability of ~30 Ma periodicity in the thermal boundary layer (D″) at the base of the Earth's mantle as cause of the mantle plumes. Consequently, the development of mantle plumes may lead to episodes of strong continental and oceanic volcanic activity, changes in the ocean chemistry, circulation and oxygenation, and finally major extinction events. Recent studies (Prokoph and Veizer 1999) demonstrate that a ~30 Ma periodicity is apparent in the Mesozoic $\delta^{13}C$ and $\delta^{18}O$ records of marine carbonate rocks. The deep-water PF species (Hart 1980; Brasier 1988) and benthic foraminifera (Kaiho 1998) are more greatly impacted by fluctuating oxygen minimum zones, whereas the shallow-water species are more resistant. The extinctions at the Cenomanian–Turonian and in late Santonian, which are known to coincide with black shale sedimentation events, were more severe for deep-water species.

(2) Extreme global sea-level falls, caused by orogenic events, often associated with climate cooling, provided regressions of shelf seas and thus removed niche spaces for PF species. This led to major extinction events (Hallam 1989), reduction PF-origination rate (Hart 1990), or both. Examples

Fig. 8. Graphic correlation of geological time series and events. (*a*) Global relative eustatic sea-level curve (in m), after Hardenbol et al. (1998). (*b*) Detrended relative sea-level curve derived by the subtraction of the second-order trend from the eustatic sea-level curve from the Barremian (t = 127 Ma) to recent. (*c*) Starts of eruptions of continental flood basalts (gray bars) with 2δ- error bars at 16 ± 1, 31 ± 1, 57 ± 2, 62(?), 65.6 ± 0.3, 88 ± 2, and 116 ± 2 Ma (Rampino and Caldeira 1992, Hofmann et al. 1997, Mahoney and Coffin 1997, Allegre et al. 1999) and oceanic plateau basalts (black bars) at 87–92 Ma (Kerr 1998) and 117–121 Ma (Rampino and Caldeira 1993); anoxic events (black circles) at about 121, 110, 93.5, and 84 Ma, after compilation of Rampino and Caldeira (1993); and positive $\delta^{13}C$ spike at ~56 Ma (cross), after Veizer et al. (1999). (*d*) Impact crater diameter (in km) after Grieve (1997 and personal communication, 1999). (*e*) Data from SO model from Fig. 7. (*f*) Relative PF origination (above zero) and relative PF extinction (below zero) at event levels. (*g*) changes of total number of PF species/Ma.; vertical dashed lines mark major PF extinction levels; asterisks in (*b*) and (*g*) mark correlative sea-level falls and high relative PF extinction.

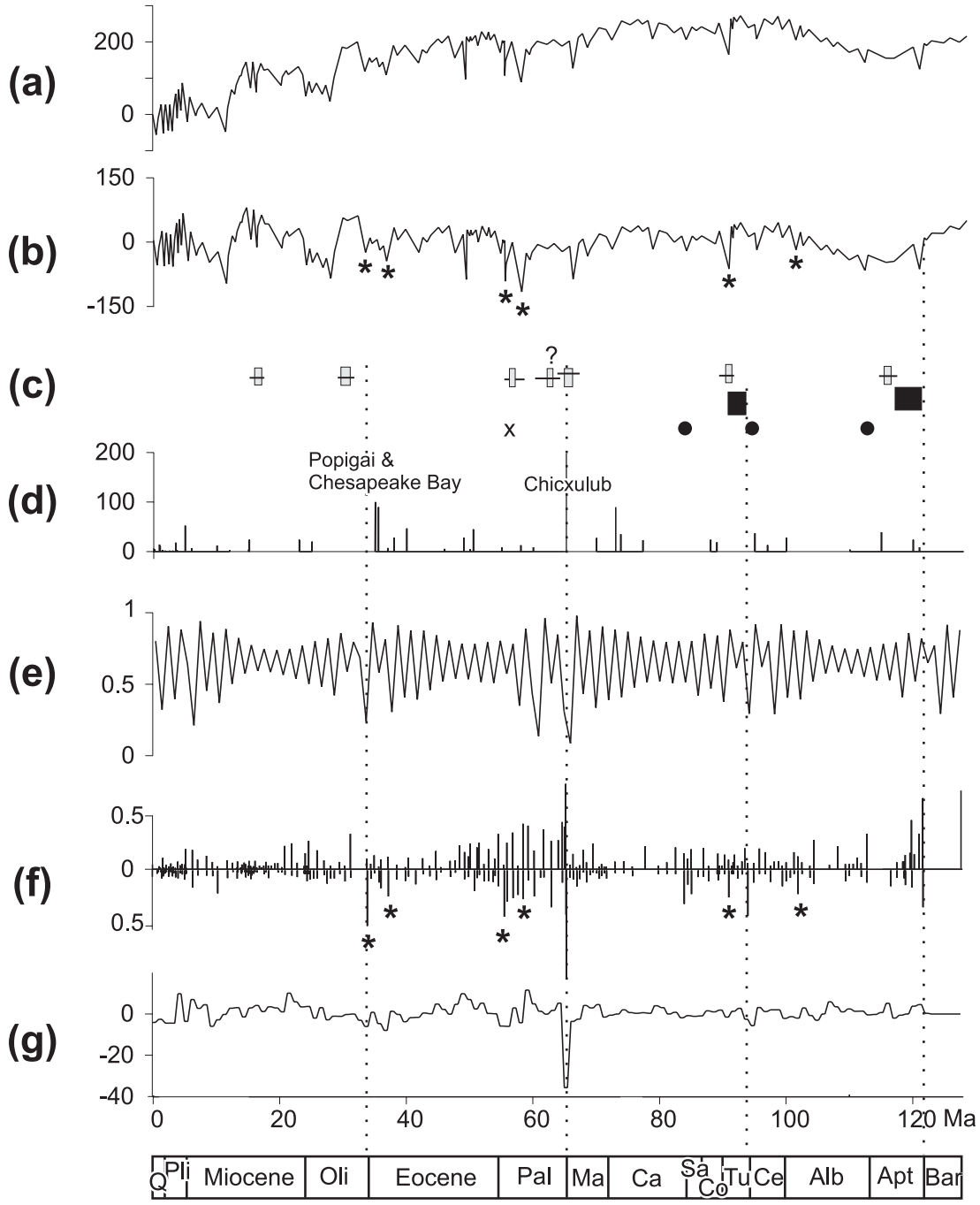

are the late Albian and late Eocene PF extinctions that corresponded with marine regressions (Hardenbol et al. 1998).

These causes, as well as other geological events (e.g., bolide impacts), may sometimes occur synchronously (e.g., Eocene–Oligocene – sea-level fall and flood basalt and K–T boundary – bolide impact and flood basalt). Consequently, our SO model and statistical results correspond with the suggestion of Rampino and Caldeira (1993) that

Fig. 9. (*a*) Wavelet analysis of (*b*) data of impact crater diameter (in km). (*c*) Detrended relative eustatic sea level with (*d*) its wavelet analysis. Time scale after Gradstein and Ogg (1996). Dashed line shows K–T boundary.

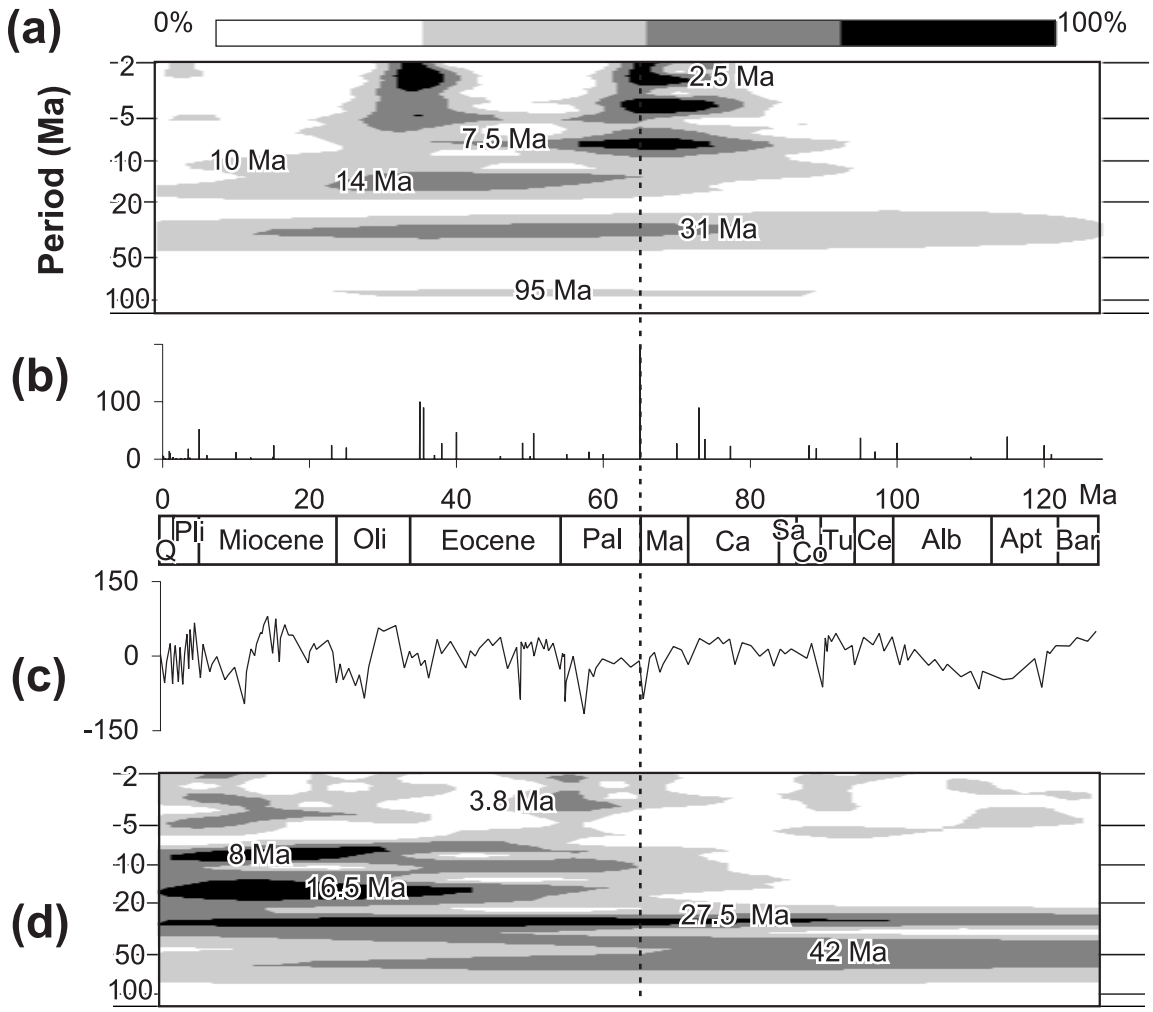

possible multiple, but interconnected, intraterrestrial events may cause extinction with a roughly 30 Ma periodicity. The nonstationary, high-frequency periods (~2.4–15 Ma) in the PF record and in our SO model may indicate that an increased rate of evolution existed during increased environmental stress, a result found in other nonlinear models (e.g., Chiba 1998; Plotnick and McKinney 1993). The driving periodicity of our SO model is phase shifted in the output, because of the coupling with a nonlinear function. Global sea-level fluctuations are similarly phase shifted, leading to the possibility that sea level may itself be part of a nonlinear system that in part controls abundance of PF species by varying the amount of available niche space.

Conclusion

Wavelet analysis quantitatively demonstrates that the PF record, particularly relative PF-extinction rates, is characterized by a ~30 Ma periodicity, slightly longer than the 26–30 Ma mass-extinction record of Phanerozoic genera and families. This periodicity is superimposed by a weak 80–100 Ma secular trend with a peak around the K–T boundary. Nonstationary periodicity of 2.4–14 Ma appears in the PF record, especially in times of increased origination and extinction rates (e.g., Paleocene, Turonian).

Self-organization in the PF record is characterized by the fast rebound of the baseline number of species after extreme extinctions (e.g., Turonian, Paleocene) and corresponds to nonstationary, high-frequency periodicity. A simple data-driven nonlinear model based on 30 Ma and a weak 100 Ma periodic forcing of the logistic map was constructed. Its output is self-organized, and its three degrees of freedom resembles essential parts the actual PF record. These singularities (i.e., K–T boundary), nonstationarities, and extrema in relative PF extinction at the Cenomanian–Turonian, and Eocene–Oligocene boundaries, which are phase shifted due to the forcing function of the SO model. This simple model can neither explain all patterns in the PF record, including short-term changes; the total PF diversity; and stochastic processes involved in the PF evolution.

Statistical analysis (correlation analysis, cross-spectral analysis) suggests that there is no single external cause for the 30 Ma and other periodicities. The correspondence of some extraordinary high relative PF extinction events with some continental and oceanic flood-basalt volcanism, global sea-level falls, global anoxic events, but only three large

Fig. 10. Cross-spectral analyses of relative PF-extinction data with impact crater diameter (solid line) and relative PF extinction with detrended relative sea level (dashed lines) for averaged data interval = 1 Ma. (*a*) Cross-amplitude, (*b*) phase spectra. Vertical solid lines at 10, 7.5, and 2.5 Ma mark correlative periodicities to relative PF extinction.

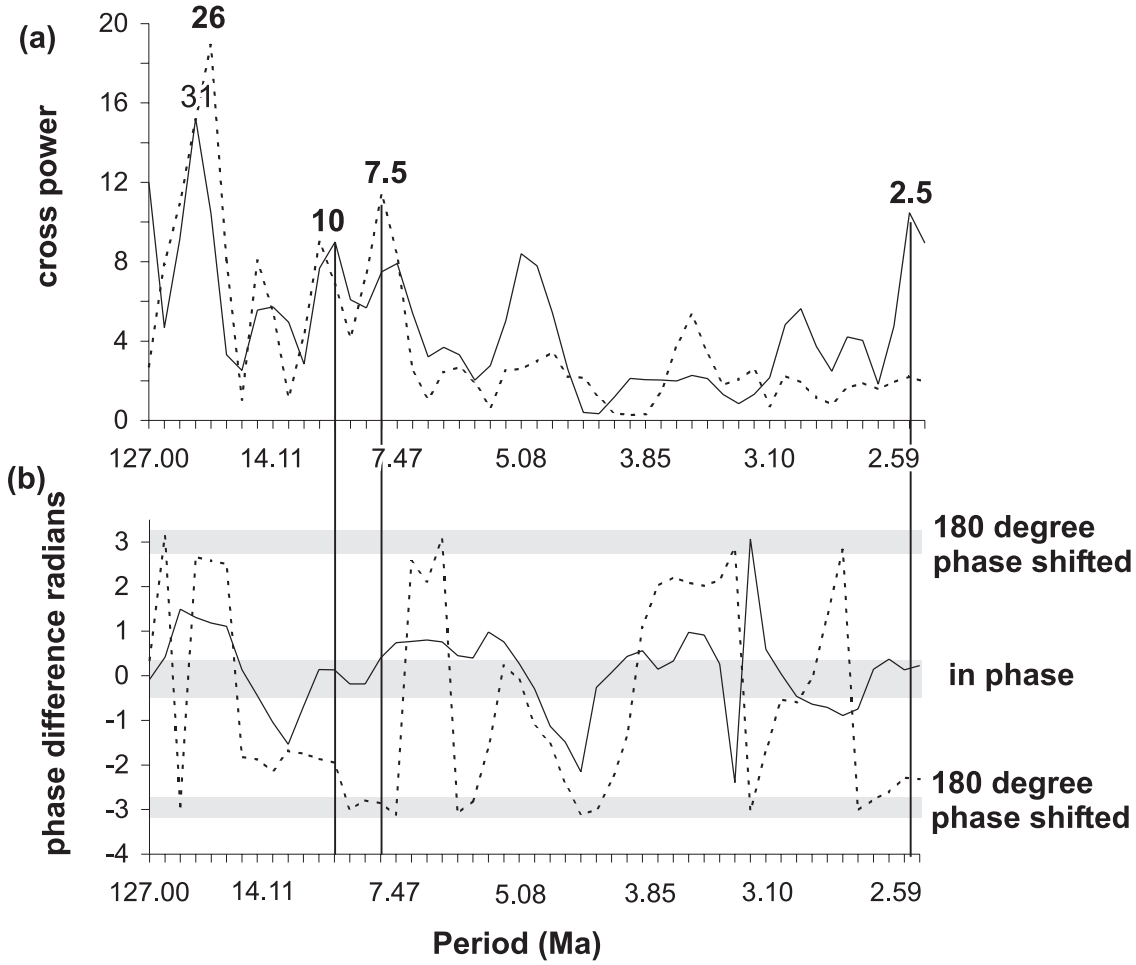

bolides (K–T boundary and in late Eocene) indicates multiple interacting, mostly terrestrial, causes for long-term periodicity in the evolution of planktic foraminifera.

Acknowledgments

We acknowledge the financial support of the Natural Sciences and Engineering Research Council of Canada (NSERC) and the donors of the American Chemical Society Petroleum Research Fund. We thank Michael Rampino and Felix Gradstein for their constructive reviews.

References

Agterberg, F.P. 1994. Estimation of the geological time scale. Mathematical Geology, **26**: 857–876.

Allegre, C.J., Birck, J.L., Capmas, F., and Courtillot, V. 1999. Age of the Deccan traps using ^{187}Re–^{187}Os systematics. Earth and Planetary Science Letters, **170**: 197–204.

Alvarez, W., Alvarez, L.W., Asaro, F., and Michel, H.V. 1982. Iridium anomaly approximately synchronous with terminal Eocene extinction. Science (Washington, D.C.), **216**: 886–888.

Asaro, F., Alvarez, L.W., Alvarez, W., and Michel, H.V. 1982. Geochemical anomalies near the Eocene/Oligocene and Permian/Triassic boundaries. Geological Society of America, Special paper 190, pp. 517–528.

Bak, P., and Sneppen, K. 1993. Punctuated equilibrium and criticality in a simple model of evolution. Physical Review Letters, **71**: 4083–4086.

Bak, P., Tang, C., and Wiesenfeld, K. 1988. Self-organized criticality. Physical Review, **A38**: 364–374.

Banerjee, A., and Boyajian, G.E. 1997. Selectivity of foraminiferal extinction in the late Eocene. Paleobiology, **23**: 347–357.

Bartlett, M.S. 1966. An introduction to stochastic processes. Cambridge, Cambridge University Press, Cambridge, U.K.

Benton, M.J. 1995. Diversification and extinction in the history of life. Science (Washington, D.C.), **268**: 52–58.

Berggren, W.A., and Casey, R.E. 1983. Introduction to the symposium on tempo and mode of evolution from micropaleontological data. Paleobiology, **9**: 326.

Bolli, H.M., Saunders, J.B., and Perch-Nielsen, K. (*Editors*). 1989. Plankton stratigraphy. Cambridge University Press, Cambridge, U.K., Vol. 1.

Bolton, E.W., Maasch, K.A., and Lilly, J.M. 1995. A wavelet analysis of Plio-Pleistocene climate indicators: A new view of periodicity evolution. Geophysical Research Letters, **22**: 2753–2756.

Brasier, M.D. 1988. Foraminiferid extinction and ecological collapse during global biological events. *In* Extinction and survival

in the fossil record. *Edited by* G.P. Larwood. Systematics Association Special Vol. 34, pp. 37–64.

Chao, B.F., and Naito, I. 1995. Wavelet-analysis provides a new tool for studying Earth's rotation. EOS, **76**: 161, 164–165.

Chiba, S. 1998. A mathematical model for long-term patterns of evolution: effects of environmental stability and instability on macroevolutionary patterns and mass extinctions. Paleobiology, **24**: 336–348.

Darwin, C. 1859. On the origin of species. Murray, London.

Davis, J.R. 1986. Statistics and Data Analysis in Geology. Wiley, New York.

Eldredge, N., and Gould, J.S. 1972. Punctuated equilibrium: an alternative to phyletic gradualism. *In* Models in paleobiology. *Edited by* T. Schopf. Freeman, Cooper, San Francisco, Calif., pp. 82–115.

Ellis, B.F., and Messina, A. 1940. Catalogue of foraminifera. American Museum of Natural History, New York (30 volumes).

Feigenbaum, M.J. 1978. Quantitative universality for a class of nonlinear transformations. Journal of Statistical Physics, **19**: 25–32.

Fischer, D.A., and Koerner, R.M. 1994. Signal and noise in four ice-core records from the Agassiz Ice Cap, Ellesmere Island, Canada: details of the last millennium for stable isotopes, melt and solid conductivity. The Holocene, **4**: 113–120.

Glikson, A.Y. 1999. Oceanic mega-impacts and crustal evolution. Geology, **27**: 387–390.

Gradstein, F.M., and Ogg, J.G. 1996. A Phanerozoic time scale. Episodes, **19**: 1–2.

Grieve, R.A.F. 1997. Extraterrestrial impact events: the record in the rocks and the stratigraphic column. Paleogeography, Palaeoclimatology, Palaeoecology, **132**: 5–23.

Grossman, A., and Morlet, J. 1984. Decomposition of Hardy functions into square integrable wavelets of constant shape. SIAM Journal of Mathematical Analysis, **15**: 732–736.

Hallam, A. 1989. The case for sea-level change as a dominant causal factor in mass extinction of marine invertebrates. Philosophical Transactions of the Royal Society of London, **B325**: 437–455.

Hardenbol, J., Thierry, J., Farley, M.B., Jaquin, T., de Graciansky, P.-C., and Vail, P.R. 1998. Mesozoic and Cenozoic Sequence Chronostratigraphic Chart. *In* Mesozioc–Cenozoic sequence stratigraphy of European basins. *Edited by* P.-C. de Graciansky, J. Hardenbol, T. Jacquin, and P. Vail. Society of Economic Paleontologists and Mineralogists (SEPM), Special Publication 60.

Hart, M.B. 1980. A water depth model for the evolution of the evolution of the planktonic foraminifera. Nature (London), **286**: 252–254.

Hart, M.B. 1990. Major evolutionary radiations of the planktonic foraminiferida. *In* Major evolutionary radiations. *Edited by* P.D. Taylor and G.P. Larwood. Systematics Association Special Vol. 42, pp. 59–72.

Hoffman, A. 1985. Patterns of family extinction depend on definition and timescale. Nature (London), **315**: 659–662.

Hoffman, A. 1989. Mass extinction: the view of a sceptic. Journal of the Geological Society London, **146**: 21–35.

Hofmann, C., Courtillot, V., Feraud, G., Rochette, P., Yirgus, G., Ketefo, E., and Pik. R. 1997. Timing of the Ethiopian flood basalt event and implications for plume birth and global change. Nature (London), **389**: 838–841.

Huismann, J. And Weissing, F.J. 1999. Biodiversity of plankton by species oscillations and chaos. Nature (London), **402**: 407–410.

Kaiho, K. 1998. Global climatic forcing of deep-sea benthic foraminiferal test size during the past 120 m.y. Geology, **26**: 491–494.

Kaiho, K., and Lamolda, M.A. 1998. Catastrophic extinction of planktonic foraminifera at the Cretaceous–Tertiary boundary evidenced by stable isotopes and foraminiferal abundance at Caravaca, Spain. Geology, **27**: 355–358.

Kauffman, S.A. 1993. The origins of order: Self-organization and selection in evolution. Oxford University Press, New York.

Kennett, J.P., and Srinivasan, M.S. 1983. Neogene planktonic foraminifera: A phylogenetic atlas. Hutchinson Ross, Stroudsburg, Pa.

Kerr, A.C. 1998. Oceanic plateau formation: a cause of mass extinction and black shale deposition around the Cenomanian–Turonian boundary? Journal Geological Society London, **155**: 619–626.

Kitchell, J.A., and Estabrook, G. 1986. Was there 26-Ma periodicity of extinction (response). Nature (London), **321**: 534–535.

Lasaga, A.C. 1998. Kinetic theory in the Earth Sciences. Princeton Series in Geochemistry, Princeton University Press, Princeton, N.J.

Loper, D.E., McCartney, K., and Buzyna, G. 1988. A model of correlated episodicity in magnetic-field reversals, climate, and mass extinctions. Journal of Geology, **96**: 1–15.

Luderer, F, and Kuhnt, W. 1997. A high resolution record of the Rotalipora extinction n laminated organic-carbon rich limestones of the Tarfaya Atlantic Coastal Basin (Morocco). Annales de la Société Géologique du Nord, **5**: 199–205.

MacLeod, N., and Keller, G. 1994. Comparative biogeographic analysis of planktic foraminiferal survivorship across the Cretaceous/Tertiary (K/T) boundary. Paleobiology, **20**: 273–287.

Mahoney, J.J., and Coffin, M.F. 1997. Large Igneous Provinces: Continental, Oceanic and, Planetary Flood Volcanism. American Geophysical Union (AGU), Geophysical Monograph, **100**.

Mann, M.E., and Lees, J.M. 1996. Robust estimation of background noise and signal detection in climatic time series. Climatic change, **33**: 409–445.

Matsumoto, M., and Kubotani, H. 1996. A statistical test for correlation between crater formation rate and mass extinctions. Monthly Notices Royal Astronomical Society, **282**: 1407–1412.

May, R.M. 1976. Simple mathematical models with very complicated dynamics. Nature (London), **261**: 459–467.

Miller, W. 1996. Ecology of coordinated stasis. Palaeogeography, Palaeoclimatology, Palaeoecology, **127**: 177–190.

Newman, M.E.J., and Sibani, P. 1999. Extinction, diversity and survivorship of taxa in the fossil record. Proceedings of the Royal Society of London, **B266**: 1593–1599.

Obradovitch, J.D. 1993. A Cretaceous time-scale. *In* Evolution of the Western Interior Basin. *Edited by* W.G.E. Caldwell and E.G. Kauffman. Geological Association of Canada, Special Publication 39, pp. 379–396.

Palmer, A.R. 1983. The decade of North American geology 1983 geologic time scale. Geology, **11**: 503.

Patterson, C., and Smith, A.B. 1987. Is the periodicity of extinctions a taxonomic artefact? Nature (London), **330**: 248–251.

Patterson, R.T., and Fowler, A.D. 1996. Evidence of self organization in planktic foraminiferal evolution: Implications for interconnectedness of paleoecosystems. Geology, **24**: 215–218.

Pearson, P.N. 1998. Speciation and extinction asymmetries in paeontological phylogenies: vidence for evolutionary progress. Paleobiology, **24**: 305–335.

Plotnick, R., and McKinney, M. 1993. Ecosystem organization and extinction dynamics. Palaois, **8**: 202–212.

Prokoph, A., and Barthelmes, F. 1996. Detection of nonstationarities in geological time series: Wavelet transform of chaotic and cyclic sequences. Computer & Geosciences, **22**: 1097–1108.

Prokoph, A., and Veizer, J. 1999. Trends, cycles and nonstationarities in marine stable isotopes through Phanerozoic time. Chemical Geology, **161**: 225–240.

Rampino, M.R., and Caldeira, K. 1992. Episodes of terrestrial geologic activity during the past 260 million years: a qualitative approach. Celestial Mechanics and Dynamical Astronomy, **54**: 143–159.

Rampino, M.R., and Caldeira, K. 1993. Major episodes of geological change: correlations, time structure, and possible causes. Earth and Planetary Science letters, **114**: 215–227.

Rampino, M.R., and Stothers, R.B. 1984. Terrestrial mass extinctions, comentary impacts and the Sun's motion perpendicular to the galactic plane. Nature (London), **308**: 709–712.

Rampino, M.R., and Stothers, R.B. 1986. Geologic periodicities and the Galaxy. *In* The Galaxy and the Solar System. *Edited by* R. Smoluchowski, J.N. Baheall, and R.S. Matthews. University of Arizona Press, Tucson, Ariz., pp. 241–259.

Rampino, M.R., and Stothers, R.C. 1988. Flood basalt volcanism during the past 250 million years. Science (Washington, D.C.), **241**: 663–668.

Raup, D.M. 1992. Large-body impact and extinction in the Phanerozoic. Paleobiology, **18**: 80–88.

Raup, D.M., and Sepkoski, J.J., Jr. 1984. Periodicity of extinctions in the geologic past. Proceedings of the National Academy of Sciences, U.S.A. **81**: 801–805.

Raup, D.M., and Sepkoski, J.J., Jr. 1986. Periodic extinctions of families and genera. Science (Washington, D.C.), **231**: 833–836.

Raup, D.M., and Sepkoski, J.J., Jr. 1988. Testing for periodicity of extinction. Science (Washington, D.C.), **241**: 94–96.

Schlanger, S.O., and Jenkins, H.C. 1976. Cretaceous anoxic events: causes and consequences. Geologie en Mjinbouw, **55**: 179–184.

Schwarzacher, W. 1993. Cyclostratigraphy and Milankovitch Theory. Developments in Sedimentology, Elsevier, Amsterdam, **52**.

Sepkoski, J.J., Jr. 1989. Periodicity in extinction and the problem of catastrophism in the history of life. Journal of the Geological Society London, **146**: 7–19.

Sepkoski, J.J., Jr. 1998. Rates of speciation in the fossil record. Philosophical Transactions of the Royal Society London, **B 353**: 315–326.

Signor, P.W., and Lipps, J.H. 1982. Sampling bias, gradual extinction patterns and catastrophes in the fossil record. Geological Society of America, Special Papers **190**: 291–296.

Sole, R.V., Manrubia, S.C., Benton, M., and Bak, P. 1997. Self-similarity of extinction statistics in the fossil record. Nature (London), **388**: 764–767.

Stigler, S.M., and Wagner, M.J. 1988. Testing for periodicity of extinction (response). Science (Washington, D.C.), **241**: 96–99.

Stothers, R.B. 1986. Periodicity of the Earth's magnetic reversals. Nature (London), **322**: 444–446.

Stothers, R.B. 1993. Flood basalts and extinction events. Geophysical Research Letters, **20**: 1399–1402.

Veizer, J., Ala, D., Azmy, K., Bruckschen, P., Buhl, D., Bruhn, F., Carden, G.A.F., Diener, A., Ebneth, S., Goddéris, Y., Jasper, T., Korte, C., Pawellek, F., Podlaha, O.G., and Strauss, H. 1999. $^{87}Sr/^{86}Sr$, $\delta^{13}C$ and $\delta^{18}O$ evolution of Phanerozoic seawater. Chemical Geology, **161**: 59–88.

Yabushita, S. 1998. A statistical test of correlations and periodicities in the geological records. Celestial Mechanics and Dynamical Astronomy, **69**: 31–48.